ARTICLE NO. 78-1210

Three-Dimensional Supersonic Interacting Turbulent Flow along a Corner

J. S. Shang* and W. L. Hankey†
Air Force Flight Dynamics Laboratory, Wright-Patterson Air Force Base, Ohio

and

J. S. Petty‡
Air Force Aero Propulsion Laboratory, Wright-Patterson Air Force Base, Ohio

The numerical solution of a three-dimensional laminar-transitional-turbulent flow along a symmetric corner was obtained for the Navier-Stokes equations using a modified Gessner's turbulence model. The specific case examined was the symmetric corner formed by the intersection of two wedges with identical wedge angles of 9.48 deg at a Mach number of 3, with the Reynolds number spanning a range from 0.4×10^6 to 1.1×10^6 for which experimental data existed. The numerical resuits duplicated all of the essential experimental observations. The present investigation seems to indicate that careful application of a turbulent eddy-viscosity concept is not limited to mere two-dimensional thin shear-layer flows. Finally, the present procedure appears to offer promise for practical engineering applications.

Nomenclature

c = speed of sound
Def = deformation tensor
e = specific internal energy, $C_V T + (u^2 + v^2 + w^2)/2$
F, G, H = vector fluxes, Eq. (12)
i, j, k = indexes of the grid-point system
K = exponent in the stretched coordinates y, z
k = molecular heat conductivity
L = length scale of eddy viscosity, Eq. (7)
L_ξ, L_η, L_ζ = difference operator
M = Mach number
$\bar{n}$ = outward normal with respect to the wedge surface
p = static pressure
Pr = Prandtl number
Pr_t = turbulent Prandtl number
$\dot{q}$ = rate of heat transfer
q = magnitude of velocity
R_{ex} = Reynolds number based on running length $\rho_\infty U_\infty x/\mu\infty$
T = static temperature
t = time
U = dependent variables in vector form, Eq. (12)
$\bar{u}$ = velocity vector
u, v, w = velocity components in Cartesian frame
u_θ, u_ϕ = velocity component in spherical coordinate system
x, y, z = coordinates in Cartesian frame
x_L, y_L, z_L = length scales of Cartesian coordinates
α_d = coefficient in pressure damping terms
γ = ratio of specific heat
$\Gamma(\bar{x})$ = transition model
δ_{ij} = Kronecker delta
ϵ = eddy viscosity
ξ, η, ζ = transformed coordinate system, Eq. (11)
θ, ϕ = angular bases of spherical coordinate system
θ_W = wedge angle with respect to freestream
Λ = parameter of transition model, Eq. (10)
μ = molecular viscosity coefficient
λ = bulk viscosity coefficient
ρ = density
$\bar{\bar{\tau}}$ = stress tensor

Subscripts

∞ = property evaluated at the freestream condition
0 = stagnation condition
e = explicit differencing operator
i = implicit differencing operator

Superscripts

$(\bar{\ })$ = vector
$(\bar{\bar{\ }})$ = tensor
n = time level

Received July 6, 1978; presented as Paper 78-1210 at the AIAA 11th Fluid and Plasma Dynamics Conference, Seattle, Wash., July 10-12, 1978; revision received Jan. 30, 1979.

Index categories: Jets, Wakes, and Viscid-Inviscid Flow Interactions; Supersonic and Hypersonic Flow.

*Aerospace Engineer, Flight Mechanics Division. Member AIAA.
†Senior Scientist, Flight Mechanics Division. Member AIAA.
‡Staff Engineer. Member AIAA.

Introduction

THE ability to analyze flows along a streamwise corner is of vital interest in numerous engineering applications. Corner flows exist in fuselage wing junctions, in rectangular inlet diffusers and ducts, in the intersection of several control surfaces and in turbo-machine blade-hub junctions. Traditionally, the flowfield has been analyzed by the superpositon of a slowly varying primary flow and a transverse flow.[1-4] The transverse flow has a pronounced effect on peripheral wall shear stress distribution and heat transfer in the corner region. In a supersonic stream, the generating mechanism of the crossflow is further complicated by the intricate shock wave structure interacting with the viscous dominated region.[5-7] In essence, corner flows are characterized by strong three-dimensional inviscid-viscous interactions. The problem is amenable to solution only through the use of the Navier-Stokes equations. This observation is reflected by the significant number of recent numerical solutions obtained for corner configurations. Some of the investigations are interested only in either the shock wave

structure and the slip surface formation[8-10] or seek the asymptotic viscous solution under particular flow conditions.[11-13] Recent works[14,15] using Navier-Stokes solvers are currently under development. The major limitation of the aforementioned efforts[14,15] is that the flow remain laminar. Hung and MacCormack[16] in their most recent work have successfully obtained the first numerical solution of the three-dimensional Navier-Stokes equations for fully turbulent inviscid-viscous interactions. The corner configurations which they investigated were formed by the intersecton of wedges of different angles and a flat plate. The present analysis attempts to remove the last restriction in the study of the three-dimensional corner problem through the inclusion of a turbulence and transition model.

The specific case examined is a symmetric corner formed by the intersection of two wedges with identical wedge angles of 9.48 deg. The flowfield investigated contains a supersonic leading edge with the subsequent development of laminar, transitional, and turbulent viscous flow along the streamwise corner (Fig. 1). The experimental data[17] were collected at a Mach number of 3 with the Reynolds number spanning a range from 0.4×10^6 to 60×10^6. The experimental data displayed rather minor Reynolds number dependence, once the fully turbulent flow condition was achieved.[17] Based on the evidence from oil film flow patterns, the aforementioned condition was reached for Reynolds numbers as low as 1.1×10^6. Since the grid-point distribution for sufficient numerical resolution is far less stringent for $R_{ex}=1.1\times10^6$ than for $R_{ex}=60\times10^6$, the low limit of the tested Reynolds number matrix was used for the present analysis, and also to study details of the transition process. The numerical results are compared with the experimental measurements of surface pressure distribution, impact pressure survey, both the laminar and turbulent shock wave formation, and oil film flow pattern. The complete flowfield structure is presented in the form of density contours, crossflow velocity diagrams, axial vorticity composition, and surface shear distributions.

Analysis

Governing Equations

The equations of motion for the present analysis are the time-dependent Navier-Stokes equations in mass-averaged variables[18] for three-dimensional flows

$$\frac{\partial\rho}{\partial t}+\nabla\cdot(\rho\bar{u})=0 \tag{1}$$

$$\frac{\partial\rho\bar{u}}{\partial t}+\nabla\cdot(\rho\bar{u}\bar{u}-\bar{\bar{\tau}})=0 \tag{2}$$

$$\frac{\partial\rho e}{\partial t}+\nabla\cdot(\rho e\bar{u}-\bar{u}\cdot\bar{\bar{\tau}}+\bar{q})=0 \tag{3}$$

where the dependent variables of this system of equations identified are ρ, $\rho\bar{u}$, and ρe. The stress tensor contains components of the Reynolds stress

$$\langle\bar{\bar{\tau}}\rangle=-p\bar{\bar{I}}+\mu\,\mathrm{Def}\;\bar{u}-\tfrac{2}{3}\mu(\nabla\cdot\bar{u})\bar{\bar{I}}-\rho\langle\overline{\overline{u_iu_j}}\rangle$$

and the heat flux includes a convective term due to the turbulent motion.

$$\langle\dot{q}_i\rangle=\dot{q}_i-\rho\langle e_iu_i\rangle$$

Although the closure problem for the system of governing equations is formidable, the approach here is to seek a simple means of effecting closure to the equations of motion. To accomplish this objective, the eddy-viscosity concept is adopted. The Reynolds stress tensor is represented by the product of the eddy viscosity and the mean flow velocity gradient. The effective conductivity of heat transfer is also defined by the turbulent Prandtl number ($Pr_t=0.9$).

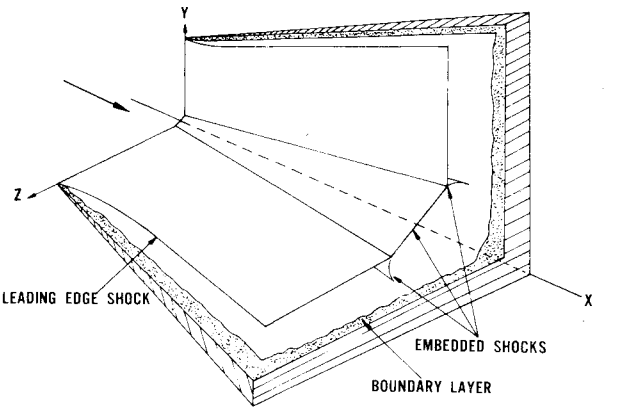

Fig. 1 Flowfield schematic.

$$\tau_{ij}=(\mu+\epsilon)(\mathrm{Def}\;\bar{u})_{ij}-[\tfrac{2}{3}(\mu+\epsilon)(\nabla\cdot\bar{u})+p]\delta_{ij} \tag{4}$$

$$\dot{q}_i=-c_p\left(\frac{\mu}{Pr}+\frac{\epsilon}{Pr_t}\right)\frac{\partial T}{\partial x_i} \tag{5}$$

The system of conservative equations reduces to the same form as that of the laminar flow counterpart. The equation of state, Sutherland's viscosity law, and assigned molecular Prandtl number (0.73) formally close the system of governing equations.

Turbulence Model

An algebraic two-layer model of the Cebeci-Smith type[19] was adopted. For the general three-dimensional problem, Prandtl[20] suggested a formulation for the flow in which neither the mean nor the turbulent motion are confined to two dimensions. The formulation is particularly suitable for flows where one component of the mean rate-of-deformation tensor is much greater than the others.

$$\epsilon=\rho(K_lL)^2\,|\mathrm{Def}\;\bar{u}|$$

where

$$|\mathrm{Def}\;\bar{u}|=\left[2\left(\frac{\partial u}{\partial x}\right)^2+2\left(\frac{\partial v}{\partial y}\right)^2+2\left(\frac{\partial w}{\partial z}\right)^2+\left(\frac{\partial v}{\partial x}+\frac{\partial u}{\partial y}\right)^2+\left(\frac{\partial w}{\partial x}+\frac{\partial u}{\partial z}\right)^2+\left(\frac{\partial w}{\partial y}+\frac{\partial v}{\partial z}\right)^2\right]^{1/2}$$

The eddy-viscosity model is a reasonable approximation provided that the rate of strain is fairly small and the deviation of the principal axes between the Reynolds stress tensor and the strain-rate tensor also is small. Finally, the transport of turbulence should not depend strongly on its past history. In spite of these seemingly overwhelming limitations, the single eddy-viscosity concept has been successfully applied to a wide class of aerodynamic problems with engineering accuracy.[21]

In the present analysis, the two-layer eddy-viscosity model is given as

Inner layer

$$\epsilon_i=\rho(K_lL)^2\left\{1-\exp\left[-\left(\frac{\rho\,|\partial q/\partial n|\,L^2}{\mu}\right)^{1/2}/26\right]\right\}^2\left|\frac{\partial q}{\partial n}\right| \tag{6}$$

where K_l is von Karman's constant (0.40) and $|\partial q/\partial n|=|\bar{n}\cdot\nabla\bar{u}|$ is preferred over the mean rate-of-

deformation. The basic relationale is that, at a large distance from the corner region, the flowfield approaches the two-dimensional wedge solution[19] while retaining symmetry with respect to the bisector of the corner. In addition, the mean rate-of-deformation reduces nearly to $|\partial q/\partial n|$ for the present problem. The eddy-viscosity coefficient along the bisector is easily determined by insisting that it satisfy the symmetry condition. Van Driest's damping factor is also contained in the inner layer model to satisfy the modified law of the wall.

The length scale used in the present formulation is the asymptotic form given by Gessner[21] for a rectangular duct. In its most basic form, the length scale can be expressed as the Buleev integral[22]

$$\frac{1}{L}=\frac{1}{2}\int_0^{2\pi}\frac{\mathrm{d}\phi}{S}$$

where ϕ is the peripheral angle of a sweep ray originating from any point (x,y,z) inside the duct, and S is the linear distance between the point and its intersection of the corner surface. Gessner[21] obtained the length scale as follows for a square duct with side dimension equal to a:

$$L=2yz(2a-y)(2a-z)/\{yz[(2a-y)^2+(2a-z)^2]^{1/2}+y(2a-z)[(2a-y)^2+z^2]^{1/2}+(2a-y)z[y^2+(2a-z)^2]^{1/2}+(2a-y)(2a-z)[y^2+z^2]^{1/2}\}$$

For the present problem of an open corner, $y/a,\ z/a\ll 1$. Thus, the length scale L acquires its asymptotic form

$$L=2yz/[y+z+(y^2+z^2)^{1/2}] \tag{7}$$

At locations sufficiently far from the corner the inner layer model reduces to the identical form previously used for the compression ramp configuration.[19]

In the law of the wake region, the outer layer model is simply the velocity defect formulation.[19] However, the definition of the kinematic boundary-layer thickness δ_i^* necessary in this formulation is ambiguous, particularly within the corner region, where the embedded shock wave system is encountered. In the present analysis the outer layer model is given as

Outer layer

$$\epsilon_0=\rho K_2 q_{\max}\int_0^{\eta_{\max}}(1-q/q_{\max})\mathrm{d}\eta \tag{8}$$

where $q=(u^2+v^2+w^2)^{1/2}$ and $K_2=0.0168$. $\eta_{\max}$ is the maximum dimension along the transformed Y coordinate direction.

In order to describe the transitional phenomena for the present problem, the transitional mode of Dhawan and Narasimha[23] was extended to three dimensions. This model is entirely empirical and requires specification of the zone of transition with a specific onset point. Nevertheless, the transition model has been adequately verified[24,25] for engineering purposes. Dhawan and Narasimha's laminar-turbulent transition model can be given as

$$\Gamma(\bar{x})=1-\exp(-0.412\bar{x}^2) \tag{9}$$

where

$$\bar{x}=(x-x_{t,i})/\Lambda,\qquad x_{t,i}\le x\le x_{t,f}$$

The parameter Λ is a measure of the extent of the transition region defined by

$$\Lambda=(x_{\Gamma=3/4}-x_{\Gamma=1/4}) \tag{10a}$$

$$\Lambda\doteq 2.0x_{t,i} \tag{10b}$$

According to a substantial amount of experimental data, the Reynolds number at the end of the transition region is roughly twice the value at the beginning of transition.[24] This experimental observation was incorporated into the transition model. Therefore, the only input required for this model was the location of the onset of transition. For the present case, the location was estimated to be 5.33 cm from the leading edge, based upon the experimental observations.[17]

Boundary Conditions and Coordinate Systems

The coordinate system selected can be described by a generating ray originating at a point upstream of the apex of the intersecting wedges. The coordinates form a surface-oriented conical system with suitable coordinate stretching to resolve the viscous-dominated region. For the present coordinate system, the origin of the transformed coordinate was located 1.27 cm upstream of the leading edges of the corner along the extended line of interception. The coordinate system used is given as follows:

$$\xi=x/x_L \tag{11a}$$

$$\eta=\left(\frac{1}{K}\right)\ell n\left\{1+(e^K-1)\left(\frac{y}{x}-\frac{\tan\theta w}{y_L}\right)\right\} \tag{11b}$$

$$\zeta=\left(\frac{1}{K}\right)\ell n\left\{1+(e^K-1)\left(\frac{z}{x}-\frac{\tan\theta w}{z_L}\right)\right\} \tag{11c}$$

where K was uniquely determined by the minimum step size in y and z and number of grid points used. For the present investigation, $\Delta y_{\min}=\Delta z_{\min}=0.3RL/\sqrt{Re_\infty}$ or $\Delta y_{\min}=\Delta z_{\min}=0.0048$ cm, the exponential stretching parameter, K attained a value of 3.3 for the grid-point system of (17,33,33). The grid spacing in the streamwise direction is constant and has a value of 0.79 cm. In order to attain the appropriate mesh size to resolve the significant features of the flowfield, the conical coordinates normal to the surface were clustered exponentially in η and ζ coordinates, and increased linearly with respect to the coordinate ξ. Therefore, the mesh steps of y and z span a range of 0.0048 to 1.34 cm. In physical space, the mesh point system traces a truncated frustum of a pyramid with maximum dimensions of $12.7\times 15.3\times 15.3$ cm (Fig. 1), but in the transformed space the computation domain is a cube.

The governing equations in the transformed space are of the following form:

$$\frac{\partial\bar{U}}{\partial t}+\xi_x\frac{\partial\bar{F}}{\partial\xi}+\left(\eta_x\frac{\partial\bar{F}}{\partial\eta}+\eta_y\frac{\partial\bar{G}}{\partial\eta}\right)+\left(\zeta_x\frac{\partial\bar{F}}{\partial\zeta}+\zeta_z\frac{\partial\bar{H}}{\partial\zeta}\right)=0 \tag{12}$$

where $\xi_x,\eta_x,\eta_y,\zeta_x,\zeta_z$ are the first-order partial derivatives of the transformed independent variables (ξ,η,ζ) with respect to the coordinates (x,y,z) of the Cartesian frame. The definition of the conventional flux vectors $\bar{F}$, $\bar{G}$, and $\bar{H}$ can be found in Ref. 15.

The associated boundary conditions for the present investigations are straightforward. Upstream, supersonic freestream conditions are prescribed. Even though the experimental evidence indicates the presence of extensive separated flow regions, far downstream the pressure distribution and surface oil film flow pattern[17] display predominantly conical flow features. Therefore, the downstream boundary conditions are assigned the asymptotic conical flow behavior.[14-16] Away from the corner region, the flow is required to approach a two-dimensional asymptote.

Initial

$$\bar{U}(0,\xi,\eta,\zeta)=\bar{U}_\infty \tag{13a}$$

Upstream

$$\bar{U}(\tau,0,\eta,\zeta)=\bar{U}_\infty \tag{13b}$$

Downstream

$$\left.\frac{\partial U}{\partial \xi}\right|_{\xi\to 1}=0 \tag{13c}$$

Two-Dimensional Asymptotes

$$\left.\frac{\partial U}{\partial \eta}\right|_{\eta\to 1}=0 \tag{13d}$$

$$\left.\frac{\partial U}{\partial \zeta}\right|_{\zeta\to 1}=0 \tag{13e}$$

On the wedge surfaces, the boundary conditions are no-slip for the velocity components and a constant surface temperature. The surface pressure is obtained by satisfying the momentum equation at the wedge surfaces. The numerical solutions for surface pressure, obtained either by satisfying this compatible condition or by assuming zero normal pressure gradient, are nearly identical.[15]

$$u=v=w=0 \qquad \text{at } \eta,\zeta=0 \tag{14a}$$

$$T_w=312\ \text{K} \qquad \text{at } \eta,\xi=0 \tag{14b}$$

$$\nabla\cdot(p\bar{\bar{I}}-\bar{\bar{\tau}}')=0 \qquad \text{at } \eta,\zeta=0 \tag{14c}$$

Numerical Procedure

The basic numerical method is the time-split or factorized scheme originated by MacCormack,[26,27] however, the numerical code also contains the option of a hybrid implicit-explicit scheme.[27] The finite-difference formulation in terms of the difference operators can be expressed as

$$\bar{U}^{n+2}=[(L_{\zeta i}L_{\zeta e})(L_{\eta i}L_{\eta e})L_\xi(L_{\eta e}L_{\eta i})(L_{\zeta e}L_{\zeta i})]\bar{U}^n \tag{15}$$

The essential idea is to solve the fluid dynamics problem by using different difference algorithms according to the locally predominate characteristics of the flowfield. Unfortunately, the present implicit scheme exhibits excessive oscillatory behavior for coarse meshes. Furthermore, the fluid dynamics phenomena investigated here are rather complex and a benchmark calculation is required to establish the validity of the eddy-viscosity model containing the approximation for laminar-turbulent transition. Therefore, the time-split explicit numerical procedure was used.

Flows containing strong shock waves often cause numerical oscillations. A numerical smoothing scheme was incorporated into the present numerical procedure. The fourth-order pressure damping suggested by MacCormack[14,16,26] was adopted with modification. The net result is an artificial viscosity-like term of the form

$$-\alpha_d\Delta t\Delta\xi_i^3\frac{\partial}{\partial\xi_i}\left[\frac{|u_i|+c}{4p}\frac{\partial^2 p}{\partial\xi_i^2}\right]\frac{\partial U}{\partial\xi_i} \qquad i=1,2,3$$

added to the difference equations. The pressure damping terms are reduced to MacCormack's expression for Cartesian coordinates. The coefficient α_d was assigned a value of 1.75 for all numerical sweep directions for the present calculations. These damping terms are effective only in the presence of shock waves.

Although to date no completely satisfactory stability analysis has been performed for the finite-difference formulation of the nonlinear Navier-Stokes equations, the following stability criterion was found to be adequate for the present purpose

$$\Delta t_i=\Delta x_i\Big/\left\{|u_i|+c+\left[\frac{2k}{\rho\Delta x_i C_p}+\frac{(\mu\lambda)^{1/2}}{\rho(\Delta x_j+\Delta x_k)}\right]\right\} \tag{16}$$

Where the indices i,j,k designate the directional alignment, i.e., $x_i\equiv x$, $x_j\equiv y$, $x_k\equiv z$, etc. Two mesh-point distributions were used for the present analysis. The preliminary result was first obtained by a $(8\times23\times23)$ system mainly to evaluate the eddy-viscosity model on a CDC Cyber 74 computer. The finer resolution calculations $(17\times33\times33)$ were performed both on the CDC 7600 computer of NASA Ames Research Center and a CDC Cyber 74 computer. The rate of data processing is 0.00748 and 0.00145 s per grid point per time step on the Cyber 74 and the CDC 7600, respectively. The two time-level-dependent variables and seven spatial transformation derivatives required a core storage of 615,600 octal words, which exceeded the capability of the Cyber 74 computer. This limitation was remedied by organizing the data according to its streamwise location into planar storage (pages) through a data manager subroutine. Only the data in process were brought into the central memory core, while the remainder were retained on a random access disk file. For the present analysis three pages of corrected level dependent variables, four pages of predicted level dependent variables, and two pages of transfomation derivatives were required to process a planar sweep. The data manager reduces the maximum core storage requirement from 615,600 to 235,000 octal words. The I/O time used for the present calculations was 1.44 times the CP time. Further reduction either in memory requirement or I/O time can be achieved by restricting the finite-difference operator sequence.

The numerical solution is considered to have reached its steady-state asymptote when the difference between two consecutive time levels of the static pressure in the strong interacting zone is less than 0.2%. The time to satisfy this criterion is nominally 4.3 times the value of the characteristic time, t_{ch}. The characteristic time is defined as the time interval required for a fluid particle to travel over the chord length ($R_L=12.68$ cm) at freestream speed ($t_{ch}=0.000206$ s).

Discussion of Results

The numerical results are presented in two groups. In the first, a direct comparison is performed of the numerical results with the experimental data. The second group illustrates the detailed structure of the corner flow. The shock wave system, slip surfaces, and vorticity distribution are presented together with the secondary flow velocity components. The surface shear stress distribution and the limiting streamline of three-dimensional flow separation[28,29] are also presented.

The shock wave structure of the entire flowfield in terms of density contours is given in Fig. 2. A total of 18 equal-increment levels of density covering the range from the freestream value to the highest value in the corner region have been plotted for each streamwise plane. One observes the intersecting shock waves due to the wedges and a set of two triple points formed by further intersection of the embedded shock waves. Secondary features such as the slip surfaces are also observable in some of these density contours. As the flow progresses downstream, undergoing transition from laminar to turbulent, the shock wave system readjusts itself to accommodate the distinctive change in length scale. The numerical result essentially duplicates the experimental observations. In Fig. 3, two shock wave structures and the associated slip surfaces are presented for laminar ($R_{ex}=0.27\times10^6$) and turbulent ($R_{ex}=1.1\times10^6$) flows. Good agreement is observed between the computed and experimental values in the location of shock waves, triple points, and slip surfaces.[17] The numerical results show the reduction in the size of the terminating embedded lambda shock as the interaction length scale decreases from laminar to turbulent flow.

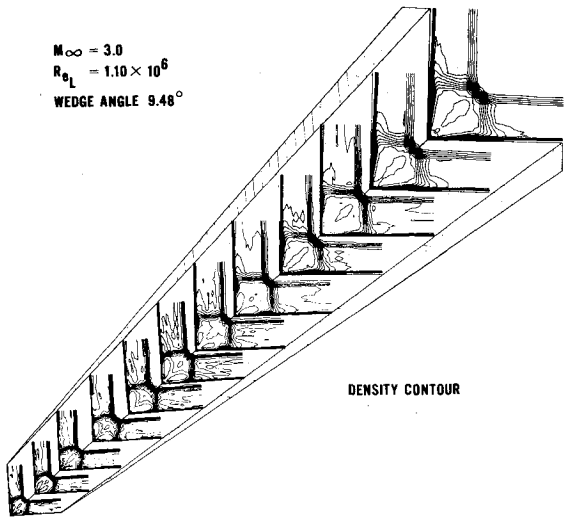

Fig. 2 Density contour for the entire field.

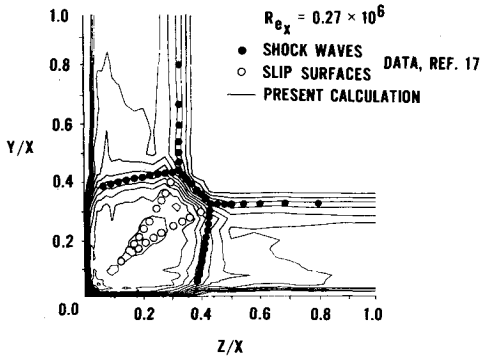

Fig. 3a Comparison of the shock wave system for laminar and turbulent flow (density contours)—laminar.

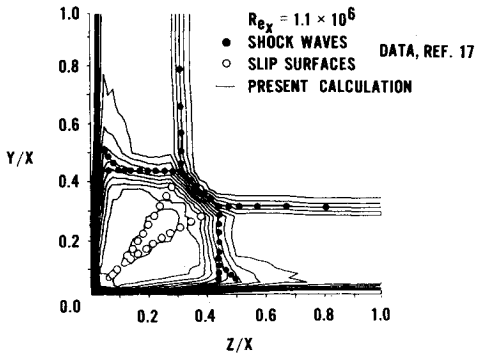

Fig. 3b Comparison of the shock wave system for laminar and turbulent flow (density contours)—turbulent.

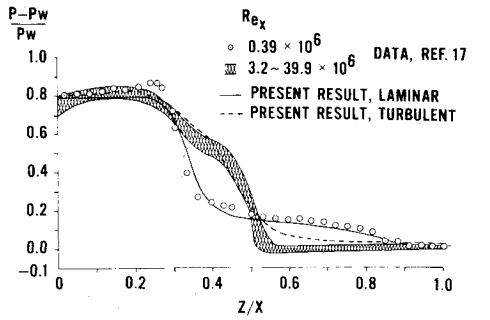

Fig. 4 Comparison of the surface pressure distribution for laminar and turbulent flow.

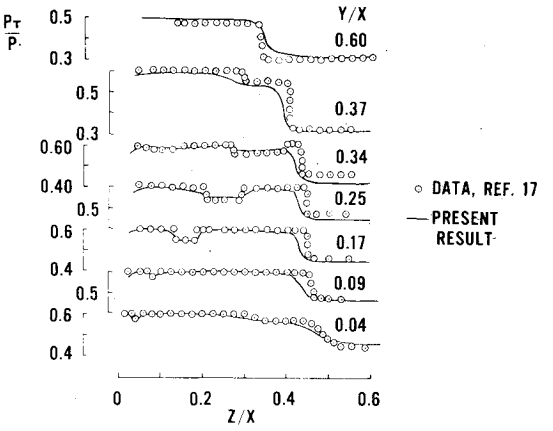

Fig. 5 Impact pressure distribution comparison.

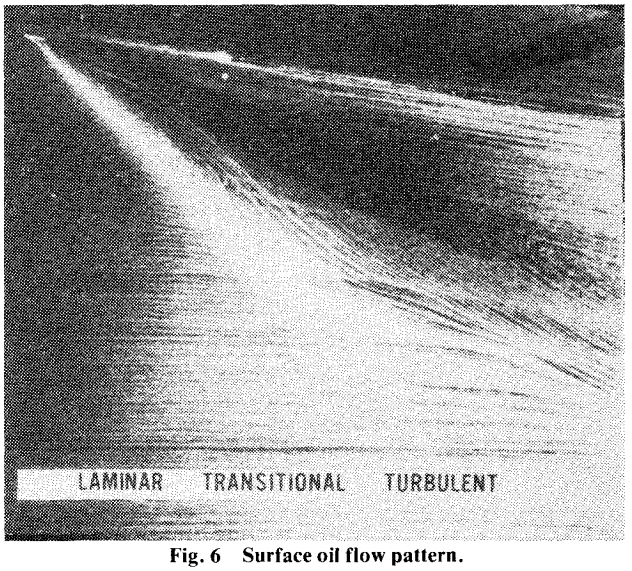

Fig. 6 Surface oil flow pattern.

In Fig. 4, surface pressure distributions for laminar and turbulent flows are presented. The agreement between the experimental measurements and calculations is excellent. The discrepancy between data and calculation is nearly confined within the scatter band of the data.[17] The maximum deviation between surface pressure data and calculation is encountered in the region from where the turbulent interaction emanates. The difference is probably caused by the numerical solution being obtained at a lower Reynolds number than the experimental condition. The computed surface pressure clearly displays the different characteristics of laminar and turbulent interacting flows while the inviscid solution fails to reveal these features.[8]

The comparison of experimental impact pressure measurements and calculated values is given in Fig. 5. The presented data were deduced from trace graphs from Ref. 17 at various heights above one wedge surface. The impact pressure distributions were normalized by the stagnation pressure. The impact pressure rises at the right-hand sides of the distribution (except for $y/x = 0.60$) mark the location of the embedded shock waves. However, in the impact pressure distribution for $x/y = 0.60$, the jump condition indicates the location of the shock wave from the other wedge. The depressions in the impact pressure distributions reflect the existence of a subsonic region bounded by slip surfaces. This cusplike triangular region is generated by the slip surfaces

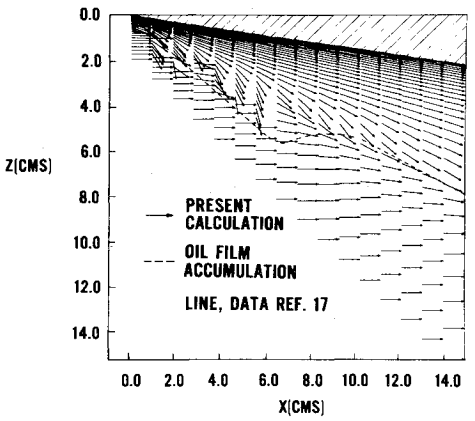

Fig. 7 Comparison of the computed surface shear force and the surface oil flow pattern.

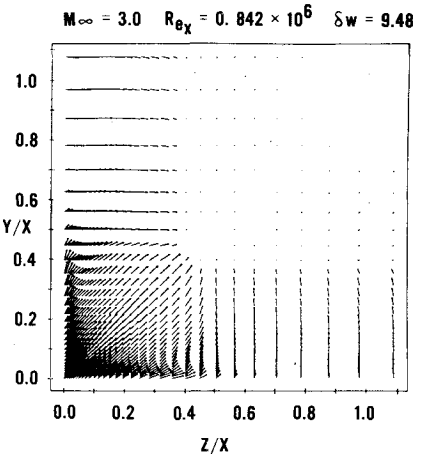

Fig. 9a Crossflow Cartesian velocity components (turbulent).

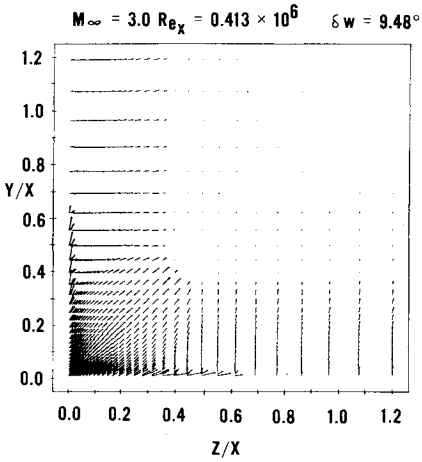

Fig. 8a Crossflow Cartesian velocity components (laminar).

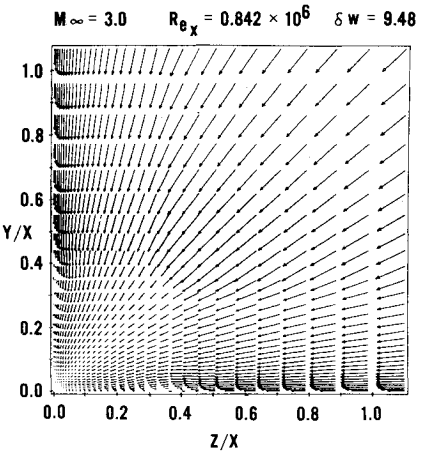

Fig. 9b Crossflow spherical velocity components (turbulent).

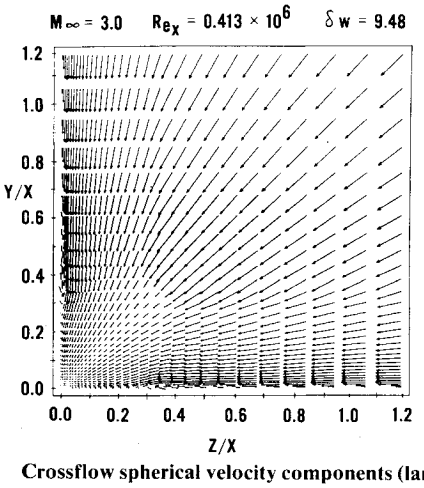

Fig. 8b Crossflow spherical velocity components (laminar).

originating at the triple points and finally merging together on the bisector of the wedge surfaces, $y/x=0.04$ (Fig. 3). The agreement between the experimental data and the calculation is remarkable in view of the rather sparse mesh point distribution.

In Fig. 6, the oil film flow pattern is presented. The S-shaped oil accumulation (separation line) indicates an orderly transition from laminar flow near the leading edge to fully developed turbulent flow downstream. According to the limiting line theory[28,29] for three-dimensional flow separation, the convergence of oil film streaks represents the separation streamline. The experiment[17] indicates that the separation is composed of two straight segments for the laminar and turbulent domains with the transition region forming an S-shaped pattern between them. These straight segments have deflection angles of 46 deg (laminar) and 32 deg (turbulent) with respect to the unperturbed freestream. The inviscid solution yields a shock wave angle of 27.4 deg due to the 10-deg wedge. The smaller difference between the separation line and shock wave angles for the turbulent flow indicates that it has a stronger resistance to flow separation under an adverse pressure gradient than does the laminar flow. The components of surface shear stress can be obtained as $\bar{f}_s=\bar{n}\cdot\bar{\bar{\tau}}$. In Fig. 7, the surface stress map is presented. However, only the orientation of the resultant stress is given. The magnitude of the surface stress changes rapidly from the leading edges of the corner to the fully turbulent flow region. The drastic change in stress magnitude from the corner to the separation line makes the graphic representation difficult. The numerical results nearly duplicate the experimental observations; the maximum deviation between the experimental data and the numerical predicted values being about 3%.

From the oil film flow pattern, surface stress map, and surface pressure distributions, one recognizes that, excluding the transition zone, the separation lines in the laminar and turbulent regions are representable by straight segments. These segments pass through the intersection of the wedges at the leading edge. Since the intersecting wedge surfaces can be defined by a generating ray, a spherical coordinate system is the most appropriate way to describe the crossflow surface.[15] According to the definition of three-dimensional

separation,[28,29] the separation is a locus of the intersection of a family of limiting streamlines. If the concept of an envelope of the limiting streamlines is adopted, the separation criterion given by Mager may be used[29]; $(\partial q_s/\partial \eta)_{\eta=0}=0$, where q_s denotes the component of the velocity in the direction perpendicular to the separation line. Fortunately, for the present investigation, the separation lines exhibit conical behavior in segments.[7,17] The velocity components in the plane perpendicular to the line of flow separation can be easily obtained by a coordinate transformation. On the surface, the segments of the separation lines coincide with the radial coordinates of the spherical coordinate system. Therefore, a surface which is orthogonal to the separation streamline is completely described by the θ and ϕ coordinates. The crossflow velocity components for laminar flow ($R_{ex}=0.413\times10^6$) and turbulent flow ($R_{ex}=0.842\times10^6$) are given in Figs. 8 and 9, respectively. In Figs. 8 and 9, the vector plots of the Cartesian velocity components v, $w(y,z)$ and the spherical velocity components u_θ, u_ϕ are both presented. The flowfield structure for the laminar is vastly different from the turbulent condition in the length scales both in the extent of flow separation and relative location of shock waves. However, similarity does exist for the general overall flowfield features for both of these flows. The major difference is the extent of separation. This observation is in agreement with Korkegi's evaluation of three-dimensional shock-induced separated flow.[7]

The crossflow plane, which is orthogonal to the separation line, carries particular significance. The Cartesian velocity components (v,w) merely reflect the displacement effects due either to the corner contour or the shock formation. The region containing the strong inviscid-viscous interaction with flow separation shows only as a region with rapid changes in v and w (Figs. 8a and 9a). However, in the spherical coordinate system the elevation and azimuthal velocity components, u_θ and u_ϕ, both lie in the surface perpendicular to the separation line and show clearly the separation phenomena. One observes in Figs. 8b and 9b the development of boundary layers on both wedge surfaces. For laminar flow, the pressure disturbance propagates outward from the embedded shock wave in the form of an adverse pressure gradient. The laminar boundary layer is known to be susceptible to even a relatively mild adverse pressure gradient. Hence, the boundary layer separates from the wedge surface (z/x, $y/x=0.85$). A strong viscous-inviscid interaction ensues, and an extensive separation region develops on both wedge surfaces as can be seen in Fig. 8b. The turbulent flow exhibits no basic difference from the laminar flow, except that the size of the separated region is substantially reduced (z/x, $y/x=0.45$). In general, the separation criterion based upon the concept of the envelope of limiting streamlines[28,29] is insufficient to be used as a precise criterion for three-dimensional separation. For the present investigation the relative orientation of the three-dimensional separation lines is known from experimental observation, and the criterion given by Mager is satisfied.[28]

Again, from Figs. 8 and 9, one observes that the inviscid region along the enveloping shock waves is indeed nearly conical; all of the velocity components converge to the geometric origin of the transverse plane. The corresponding region for the velocity components aligned with the Cartesian frame, v and w, indicates correctly the unperturbed freestream values. The shock wave location is clearly revealed by the changes in these velocity components.

The radial component of vorticity was also investigated. The numerical results show high vorticity in the viscous region, particularly in the reverse flow domains. Two self-contained vortices also evolve adjacent to the slip surfaces. Since the wedge angles are relatively small, multiple vortex formation is absent.[7,17]

In Fig. 10, the crossflow Mach number contours are presented. The shock wave envelope is again evident and remains symmetric. The crossflow sonic line is bounded by the triple point and the embedded shock waves. The penetrating inviscid finger,[15] which was observed for an asymmetric corner at a hypersonic Mach number, is completely absent. The inviscid finger has been found to be coincident with a locally high rate of heat transfer. Since the inviscid finger is absent for the investigated symmetric corner one may conclude that hot spots would not be so severe as those of asymmetric corners.

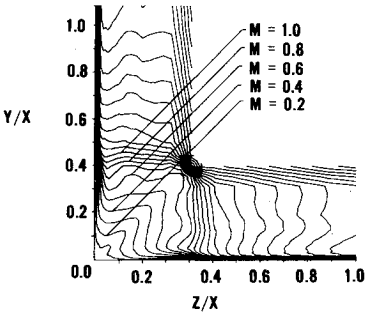

Fig. 10 Crossflow Mach number contour.

Conclusions

The numerical solution of a three-dimensional laminar-transitional-turbulent flow along a symmetric corner has been obtained. The present result duplicates nearly all of the essential experimental observations. The present numerical results substantiate the envelope of limiting lines for three-dimensional flow separation and, in particular, the criterion given by Mager.[29] In addition, the inviscid finger of an asymmetric corner can be minimized by using symmetric configurations, thus reducing the local heating load.[15] The present investigation seems to indicate that careful application of an eddy-viscosity concept is not limited to two-dimensional thin shear-layer flows. Gessner's formulation yields an adequate description of turbulence for corner flows (at least for engineering accuracy). Finally, the present procedure appears to offer promise for the analysis of inlet and fuselage-wing junction flowfields for practical engineering applications.

Acknowledgment

The authors are indebted to D.S. McRae and the NASA Ames Research Center for assistance in performing calculations on the CDC 7600 Ames computer.

References

[1] Nikuradse, J., "Untersuchungen uber die Geschwindigkeitsvereilung in Turbulenten Stromungen," Thesis, Göttingen 1926 VDI-Forschungsheft 281, Berlin, 1926.

[2] Prandtl, L., *Essentials of Fluid Dynamics*, Blackie, London, 1952.

[3] Eichelbrenner, E. A. and Preston, J. H., "On the Role of Secondary Flow in Turbulent Boundary Layers in Corners (and Salients)," *Journal de Mécanique*, Vol. 10, 1971, pp. 91-112.

[4] Gessner, F. B., "The Origin of Secondary Flow in Turbulent Flow Along a Corner," *Journal of Fluid Mechanics*, Vol. 58, 1973, pp. 1-25.

[5] Charwat, A. F. and Redekopp, L. G., "Supersonic Interference Flow Along the Corner of Intersecting Wedges," *AIAA Journal*, Vol. 5, March 1967, pp. 480-488.

[6] Cresei, R. J., Rubin, S. G., Nardo, C. T., and Lin, T. C., "Hypersonic Interaction Along a Rectangular Corner," *AIAA Journal*, Vol. 7, Dec. 1969, pp. 2241-2246.

[7] Korkegi, R. H., "On the Structure of Three-Dimensional Shock Induced Separated Flow Regions," *AIAA Journal*, Vol. 14, May 1976, pp. 597-600.

[8] Kutler, P., "Numerical Solution for the Inviscid Supersonic Flow in the Corner Formed by Two Intersecting Wedges," AIAA Paper 73-675, Palm Springs, Calif., 1973.

[9] Shankar, V. and Anderson, D. A., "Numerical Solutions for Inviscid Supersonic Corner Flows," Engineering Research Institute,

Iowa State University, Ames, Iowa, Final Rept. ISU-ERI-Ames-74090, May 1974.

[10] Shankar, V., Anderson, D., and Kulter, P., "Numerical Solutions for Supersonic Corner Flow," *Journal of Computational Physics*, Vol. 17, July 1975, pp. 160-180.

[11] Weinberg, B.C. and Rubin, S.G., "Compressions Corner Flow," *Journal of Fluid Mechanics*, Vol. 56, 1974, pp. 753-774.

[12] Ghia, K.N. and Davis, R.T., "A Study of Compressible Potential and Asymptotic Viscous Flows for Corner Regions," *AIAA Journal*, Vol. 12, 1974, pp. 355-359.

[13] Mikhail, A.G. and Ghia, K.N., "Study of Viscous Compressible Flow Along an Axial Corner," AIAA Paper 77-685, Albuquerque, N. Mex., June 27-29, 1977.

[14] Hung, C. M. and MacCormack, R. W., "Numerical Solution of Supersonic Laminar Flow Over a Three-Dimensional Compression Corner," AIAA Paper 77-694, Albuquerque, N. Mex., June 27-29, 1977.

[15] Shang, J. S. and Hankey, W. L., "Numerical Solution of the Navier-Stokes Equations for a Three-Dimensional Corner," *AIAA Journal*, Vol. 15, Nov. 1977, pp. 1575-1582.

[16] Hung, C. M. and MacCormack, R. W., "Numerical Solution of Three-Dimensional Shock Wave and Turbulent Boundary Layer Interaction," AIAA Paper 78-161, Huntsville, Ala., Jan. 16-18, 1978.

[17] West, J. E. and Korkegi, R. H., "Supersonic Interaction in the Corner of Intersecting Wedges and High Reynolds Numbers," *AIAA Journal*, Vol. 10, May 1972, pp. 652-656.

[18] Rubesin, M. W. and Rose, W. C., "The Turbulent Mean-Flow Reynolds-Stress and Heat Flux Equations in Mass-Averaged Dependent Variables," NASA TM X-62, 248, March 1973.

[19] Shang, J. S. and Hankey, W. L., "Numerical Solution for Supersonic Turbulent Flow Over a Compression Ramp," *AIAA Journal*, Vol. 13, Oct. 1975, pp. 1368-1374.

[20] Goldstein, S., Ed., *Modern Development in Fluid Dynamics*, Vol. 1, Oxford University Press, 1957, pp. 206-208.

[21] Gessner, F. B. and Po, J. K., "A Reynolds Stress Model for Turbulent Corner Flows—Part I; Comparisons Between Theory and Experiment," *Journal of Fluids Engineering, Transactions of the ASME*, Vol. 98, Ser. 1, June 1976, pp. 269-277.

[22] Buleev, H. I., "Theoretical Model of the Mechanism of Turbulent Exchange in Fluid Flows," *AERE Translation 957*, Atomic Energy Research Establishment, Harwell, England, 1963.

[23] Dhawan, S. and Narasimha, R., "Some Properties of Boundary Layer Flow During the Transition from Laminar to Turbulent Motion," *Journal of Fluid Mechanics*, Vol. 3, 1958, pp. 418-436.

[24] Shang, J. S., Hankey, W. L., and Dwoyer, D. L., "Numerical Analysis of Eddy Viscosity Models in Supersonic Turbulent Boundary Layers," *AIAA Journal*, Vol. 2, Dec. 1973, pp. 1677-1683.

[25] Shang, J. S., "Computation of Hypersonic Turbulent Boundary Layers with Heat Transfer," AIAA Paper 73-699, Palm Springs, Calif., July 16-18, 1973.

[26] MacCormack, R. W., "Numerical Solutions of the Interactions of a Shock Wave with a Laminar Boundary Layer," *Lecture Notes in Physics*, Vol. 8, Springer Verlag, New York, N.Y., 1971, p. 151.

[27] Shang, J. S., "An Implicit-Explicit Method for Solving of the Navier-Stokes Equations," *AIAA 3rd Computational Fluid Dynamics Conference*, Albuquerque, N. Mex., June 27-28, 1977, pp. 141-148.

[28] Moore, F. K., Ed., *Theory of Laminar Flows, High Speed Aerodynamics and Jet Propulsion*, Vol. IV, Princeton University Press, Princeton, N.J., 1964, pp. 387-390.

[29] Wang, K. C., "Separation of Three-Dimensional Flow," Martin Marietta Corp., MML TR-76-54C, Aug. 1976.